Research

Author for correspondence:
Brian R. Patton
e-mail: brian.patton@strath.ac.uk

THE ROYAL SOCIETY PUBLISHING

An open-source alignment method for multichannel infinite-conjugate microscopes using a ray transfer matrix analysis model

Gemma S. Cairns and Brian R. Patton

Department of Physics and SUPA, University of Strathclyde, Glasgow G4 0NG, UK

GSC, 0000-0003-0524-8008; BRP, 0000-0001-8222-4419

Multichannel, infinite-conjugate optical systems easily allow implementation of multiple image paths and imaging modes into a single microscope. Traditional optical alignment methods which rely on additional hardware are not always simple to implement, particularly in compact open-source microscope designs. We present here an alignment algorithm and process to position the lenses and cameras in a microscope using only image magnification measurements. We show that the resulting positioning accuracy is comparable to the axial resolution of the microscope. Ray transfer matrix analysis is used to model the imaging paths when the optics are both correctly and incorrectly aligned. This is used to derive the corresponding image magnifications. We can then extract information about the lens positions using simple image-based measurements to determine whether there is misalignment of the objective lens to sample distance (working distance) and with what magnitude and direction the objective lens needs to be adjusted. Using the M4All open-source 3D printable microscope system in combination with the OpenFlexure microscope, we validate the alignment method and highlight its usability. We provide the model and an example implementation of the algorithm as an open-source Jupyter Notebook.

This article is part of the Theo Murphy meeting issue 'Open, reproducible hardware for microscopy'.

1. Introduction

Advanced microscopes often include multiple optical paths in the system to enable, for example, multi-colour fluorescence microscopy and to combine multiple modes of microscopy in one instrument. There are two different ways to design an imaging path; finite-conjugate and infinite-conjugate systems. In a finite-conjugate design, the sample is positioned between f_0 and $2f_0$ before the objective lens (where f_0 is the effective focal length of the objective lens). The objective lens then focuses light at an intermediate image plane [1] where either an imaging sensor or relay lens, such as an eyepiece for direct observation, can be placed (figure 1*a*). While there are methods for allowing multiple imaging paths in a finite-conjugate system, it can be more complicated to implement than in an infinite-conjugate system.

An infinite-conjugate system positions the sample at f_0 before the objective lens and produces a collimated beam after the objective lens from a single point source in the focal plane. The collimated beam subsequently must be focused using a tube lens to form an image (figure 1*b*) [1]. To easily implement multiple imaging paths, non-focusing optics for splitting light into different detection channels, such as dichroic mirrors and beamsplitters, can be placed between the objective and tube lenses in the collimated 'infinity space' without introducing spherical aberration into the system and without changing the position of the image plane [3]. The distance between the objective and tube lens can also be varied without impacting the magnification, further easing the implementation of multichannel systems. However, there is a maximum distance that the infinity space can occupy before vignetting occurs. This can be identified by a change in the observed intensity due to the position of an object within the field of view—moving the object will see it darken as it approaches the edge of the field of view. Vignetting is due to the finite size of the optics used in any implementation of a microscope and requires thought about the physical dimensions of optical elements and apertures along the optical path to prevent or mitigate it within the required field of view. The open-source raytracing Python library [4] which we use later in this paper to carry out ray transfer matrix calculations also provides vignetting calculations and highlights the optical elements at which vignetting occurs along with the unobscured field of view. We do not carry out further discussion of vignetting within this paper, but it is well described in Noël *et al*. [4].

Note that figure 1 depicts the objective lenses as single lens elements, however in practice, objective lenses contain multiple lens elements. Therefore, f_0 is stated as an effective focal length by manufacturers and is measured from an effective plane within the objective lens body called the principle plane where refraction can be assumed to occur were the lens an ideal thin lens. This plane is not normally physically marked on the objective. Instead, objective lens manufacturers also state a working distance for the lens, which is illustrated in figure 2. For objectives designed to work with a coverslip, the working distance does not include the coverslip thickness (i.e. an objective specified to have a 400 µm working distance and working with 170 µm coverslips will have the focal plane 570 µm from the front surface of the objective). For an objective placed at the working distance from the coverslip, as in figure 2, this means that the focal plane will be coincident with the bottom surface of the coverslip.

When setting up a multichannel infinite-conjugate microscope, it is important that the objective lens—tube lens system is aligned so that the plane being imaged on the sensor is positioned at the correct working distance. If it is not, the infinity space will not be collimated, resulting in different magnifications for each channel if they have different path lengths. In addition, other aberrations and field distortions may be introduced when using the objective at the wrong working distance.

Note that collimation refers to rays emitted from a single point source at the sample focal plane being parallel in the infinity space after passing through the objective lens.
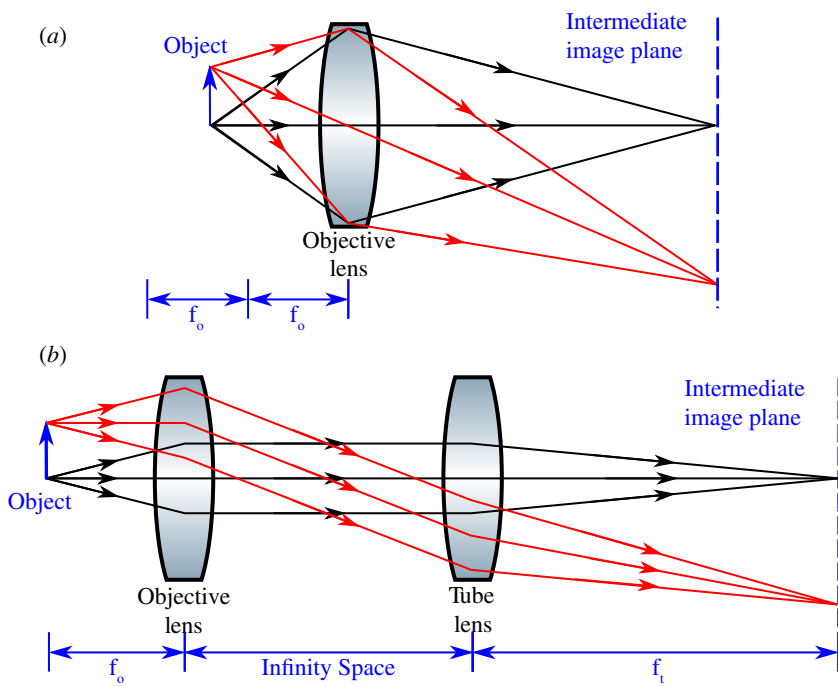
Figure 1. Optical schematics of (*a*) a finite-conjugate optical system where the sample is positioned between f_0 and $2f_0$ and the objective lens focuses and forms an image at a finite distance, and (*b*) an infinite-conjugate optical system where the sample is positioned at f_0 and the objective lens does not directly form a real image of the object, therefore a tube lens with focal length f_t must be used to focus the collimated beam. The collimated path is referred to as the infinity space. Figure from [2].
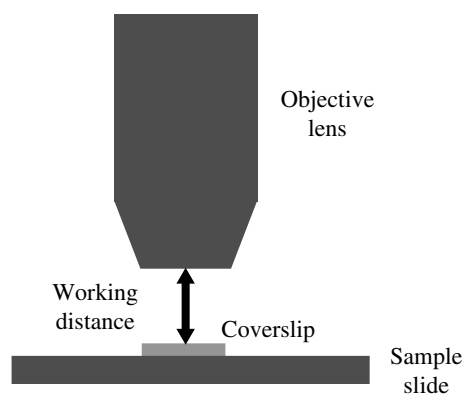

Figure 2. Illustration of the definition of the working distance of an objective lens with reference to the sample coverslip. Note that, for objectives designed to be used with a coverslip, the imaging plane in this example will be immediately under the coverslip. Figure from [2].

As can be seen in figure 1*b*, extended objects in the sample plane (red) will result in beam divergence in infinity space, as each collimated bundle of rays from each point contributing to the extended object will propagate at a different angle to the optical axis (compare the black and red ray bundles). Therefore, for microscopes that image samples with illumination spread over a wide area, collimation is not the same as looking to see if all the light rays coming out of the back of the objective remain parallel. Instead, checking whether the rays from a point source are collimated (i.e. checking that the sample is at the correct working distance in an infinite-conjugate system) must be achieved through
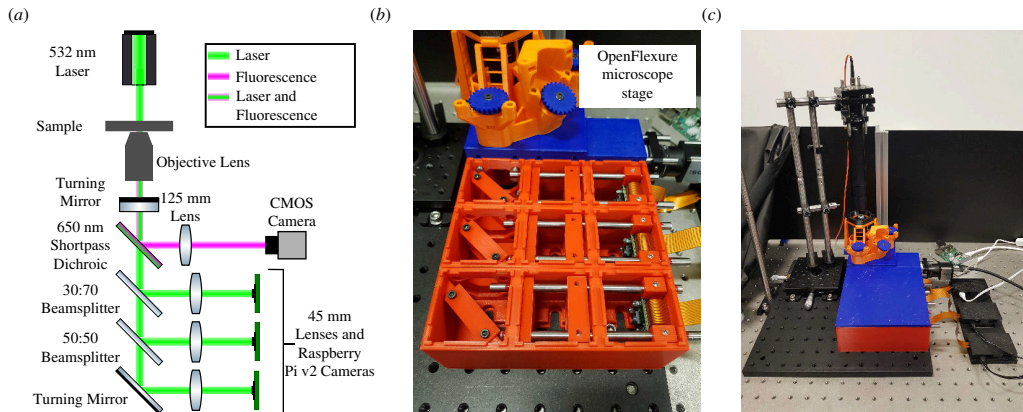
Figure 3. (*a*) Schematic of the M4All fluorescence and TIE microscope where the three brightfield channels have path lengths of $d\_total = 300$, 350 and 400 mm, respectively. (*b*) Zoomed in photo of the M4All microscope in practice in combination with the OpenFlexure microscope stage [10]. (*c*) Zoomed out photo of the overall microscope including the illumination optics and the Raspberry Pi controllers. Note that the three axes on the OpenFlexure stage were controlled using stepper motors but are not shown here. Figure adapted from [2].

an appropriate technique. Recently, there has been a growing community of researchers focused on developing open-source hardware for microscopy (see [5] for an extensive list of projects), where designs are becoming increasingly compact which results in difficulties using traditional optical alignment methods.

Such traditional methods include auto-collimators [6] and shear plates to ensure the infinity space is collimated, both of which are very effective but require dedicated hardware which may not fit into the optical path if the design is compact. Johnstone *et al.* [6] have previously highlighted that the maker of the OpenRAMAN project (an open-source Raman spectrometer) [7] has provided an excellent resource for describing the principles of an auto-collimator and how to build one [8,9]. As discussed in the introduction, if a sample is placed at the correct effective focal length/working distance of an infinity-corrected objective lens, the output from that lens will be collimated. If a mirror is placed in the collimated path to reflect the light back through the objective lens, the reflected image should be formed at the sample location if the light is perfectly collimated [9]. The example auto-collimator in Johnstone *et al.* [6] uses a light source and crosshair reticle as the object which is imaged onto a camera via reflection from a beamsplitter after propagating through the optical system to be collimated. The lens to be aligned is placed in the beam transmitted through the beamsplitter and a mirror is placed after the lens to reflect the light transmitted through the lens back to the camera in the auto-collimator. The lens is then positioned so that the image of the crosshair reflected back from the mirror is also in focus on the camera, the mirror is then at the focal plane of the lens being aligned and this information is then used when setting up the system (Johnstone *et al.* [6] give practical examples of how to do so). The auto-collimator is a large setup and is designed with the optical path parallel to an optical bench and to be used with precise optomechanics. As can be seen later in this article in figure 3, this method would not be suitable for the compact and boxed in microscope design shown here.

Similarly, a shear plate (or shearing interferometer) is an optical wedge which is positioned at 45° to the beam path [11]. It requires a light source of coherence length longer than the optical path length through the interferometer and so is typically used with a continuous wave laser. It is ineffective with incoherent sources or short-pulse duration lasers (such as many femtosecond lasers) due to this coherence requirement. Interference occurs between the reflected beams from the front and back surfaces of the shear plate. When the beam is collimated, the interference fringes are parallel to a reference line on the plate, and they are tilted if not collimated. Beyond the coherence requirements, a shear plate is a precise optical element and is usually encased in

an optomechanical mount, which again is not suitable for easily inserting and removing from a compact 3D printed microscope design.

Another common optical alignment method exists to achieve collimation which does not require additional hardware. When imaging an object at an 'infinite distance' through a single lens, the image is formed at the lens focal length [11]. Therefore, a single lens and camera combination can be focused on a distant object and fixed at the correct positions. Then, when combined with an objective lens, the objective lens will be at the correct working distance when the sample is in focus on the camera. However, because of the enclosed nature of some 3D printed microscopes, it may not be simple to remove and fix the distance of the tube lenses and cameras and insert back into the microscope.

Therefore, to align an infinite-conjugate multichannel microscope without the use of additional hardware, and without the need to image a distant object, we have developed an image-based alignment method based on a mathematical ray transfer matrix analysis (RTMA) model. The only requirements for the method are:

— To have a way of accurately controlling the z step (focusing) movements of either the sample or objective lens.
— To know the specifications of the optics and cameras in the system.
— To decide whether it is important to know the absolute magnifications of the imaging channels or whether it is adequate to know their relative magnifications to one another. This will determine whether a feature-size calibrated sample is required, e.g. a calibrated graticule slide.

In this article, we describe the mathematical model and resulting alignment method in detail before showing it being used to align a low-cost, open-source and 3D printable multichannel microscope built using a combination of two different open-source hardware projects, namely M4All (MultiModal Modular Microscopy for All) [12] and the OpenFlexure microscope stage [10]. M4All is a 3D printable and modular cube-based optomechanics system which was primarily designed to enable low-cost, stable and light-tight multichannel microscope construction. Full details can be found on the project's repository [12]. Briefly, the repository contains a suite of cube designs which are joined together according to the user's optical design in FreeCAD [13] (an open-source CAD software) and printed monolithically for enhanced stability and reduced printing errors compared to individually printed parts. The repository also contains a suite of inserts for various different optical elements and cameras. The OpenFlexure microscope stage is a 3D printable three-axis microscope stage based on plastic flexures. The stage is combined with the M4All system via a jigsaw-type connector to create a compact and virtually light-tight multichannel microscope. Further details of the multichannel microscope developed using the two projects and the alignment of the microscope will be discussed in §4 below.

2. Ray transfer matrix analysis theory

Mathematical ray tracing calculations within the paraxial approximation (where only light rays which make a small angle to the optical axis are considered, such that $sin(\theta) \approx \theta$) can be performed using RTMA. Note that in high numerical aperture ($NA = nsin(\theta)$) systems, where θ is larger, ray-tracing still often gives useful results. With this in mind, we can recommend this alignment approach even with high-NA ($NA > 0.6$) objectives. For those unaware of the theory of RTMA, Valérie Pineau *et al*. [4] provide an excellent introduction to both the theory and the Python library we use in this article.

A light ray at a plane along the optical axis z has a height y and angle θ, with respect to z which is represented as a ray vector:

$$\boldsymbol{r} = \begin{bmatrix} y \\ \theta \end{bmatrix}$$ (2.1)

In RTMA, the input ray vector is transformed through different optical elements or free space propagation paths which are described by 2 × 2 matrices, known as transfer matrices and also often referred to by their indices as ABCD matrices. The output ray vector is defined by left multiplication of the input ray vector with the transfer matrices for each element (note here that the ABCD matrix represents the transfer matrix for the total system):

$$\begin{bmatrix} y_{out} \\ \theta_{out} \end{bmatrix} = \begin{bmatrix} A & B \\ C & D \end{bmatrix} \begin{bmatrix} y_{in} \\ \theta_{in} \end{bmatrix} = \begin{bmatrix} Ay_{in} + B\theta_{in} \\ Cy_{in} + D\theta_{in} \end{bmatrix}$$ (2.2)

For this work, it is sufficient to use only the transfer matrices for free space and a thin lens, respectively, where d is the propagation distance in free space and f is the focal length of the thin lens (transfer matrices for further elements and matrix derivations can be found in Burch *et al.* [14]):

$$\begin{bmatrix} 1 & d \\ 0 & 1 \end{bmatrix}$$ (2.3)

$$\begin{bmatrix} 1 & 0 \\ -\dfrac{1}{f} & 1 \end{bmatrix}$$ (2.4)

The total ABCD matrix can be used to derive some useful properties of the system [4,14]. Most importantly for this work is the fact that when $B = 0$, the system produces a real image at the output plane from an object at the input plane. This is equivalent to y_{out} being independent of θ_{in}. The lateral and angular magnifications in this case are given by A and D, respectively.

3. Ray transfer matrix analysis model for alignment of infinite-conjugate microscope designs

The systems we wished to align comprised a single objective and an additional single tube lens per optical path, as shown in figure 4. We therefore demonstrate the application of our alignment routine for such a microscope—we anticipate that it would also work for more complex optical paths with suitable calculation of the total ABCD matrix. To model a correctly aligned microscope with an infinite-conjugate optical design, we define variables in figure 4. The total length of the channel from the sample to the camera sensor is *d_total*. Due to the design of the OpenFlexure microscope and the M4All system, we treat *d_total* as being fixed in the following for this example. The sample position on the OpenFlexure microscope stage is fixed in the axial direction and the cameras are also fixed in place within the M4All cubes—it is the objective lens which moves to focus in z as well as the tube lenses. For other systems, the total distance may change with sample positioning and this would need to be incorporated in the calculation of the total ABCD matrix. Treating the objective lens as a single thin lens, the distance between the sample and the objective lens is *d_sample*. The distance between the objective lens and the camera sensor, and the objective lens and the tube lens is *d_intercam* and *d_interlens*, respectively. Finally, we define the distance between the tube lens and the camera sensor as *d_cam*. This set of variables implies the manner in which we align the system—the sample is placed as close to the correct working distance as we can estimate by moving the objective (the sample stage is fixed in position with respect to the propagation axis), the camera is also fixed in position at *d_total* from the sample by a non-adjusting mount, and we move the tube lens to focus the image of the sample.

The defined variables, along with the objective lens effective focal length f_o and tube lens focal length f_t, can be substituted into the ABCD matrices (equations 2.3 and 2.4) to build
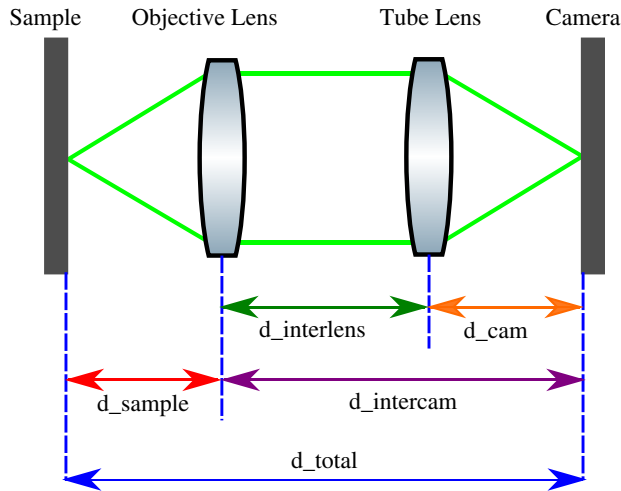
Figure 4. Simplified schematic of a single infinite-conjugate imaging channel to define variables for ray transfer matrix analysis. Figure from [2].

the matrix equation 3.1 for the infinite-conjugate imaging channel (where the matrices are left multiplied in the order they are positioned in the optical path).

$$\begin{bmatrix} y_{out} \\ \theta_{out} \end{bmatrix} = \begin{bmatrix} 1 & d\_cam \\ 0 & 1 \end{bmatrix} \begin{bmatrix} 1 & 0 \\ -\dfrac{1}{f_t} & 1 \end{bmatrix} \begin{bmatrix} 1 & d\_interlens \\ 0 & 1 \end{bmatrix} \begin{bmatrix} 1 & 0 \\ -\dfrac{1}{f_o} & 1 \end{bmatrix} \begin{bmatrix} 1 & d\_sample \\ 0 & 1 \end{bmatrix} \begin{bmatrix} y_{in} \\ \theta_{in} \end{bmatrix} \tag{3.1}$$

The following definition can also be made for d _interlens :

$$d\_interlens = d\_total - d\_sample - d\_cam \tag{3.2}$$

In a correctly aligned system, d_sample is equal to f_o and d_cam is equal to f_t. Therefore, the matrix equation becomes:

$$\begin{bmatrix} y_{out} \\ \theta_{out} \end{bmatrix} = \begin{bmatrix} 1 & f_t \\ 0 & 1 \end{bmatrix} \begin{bmatrix} 1 & 0 \\ -\dfrac{1}{f_t} & 1 \end{bmatrix} \begin{bmatrix} 1 & d\_total - f_o - f_t \\ 0 & 1 \end{bmatrix} \begin{bmatrix} 1 & 0 \\ -\dfrac{1}{f_o} & 1 \end{bmatrix} \begin{bmatrix} 1 & f_o \\ 0 & 1 \end{bmatrix} \begin{bmatrix} y_{in} \\ \theta_{in} \end{bmatrix} \tag{3.3}$$

Upon substituting the microscope design values for d_total, f_o and f_t into the matrix equation for a correctly aligned system and multiplying the transfer matrices to obtain a single transfer matrix for the total channel, the lateral magnification of the image, A, will equal the value M obtained using:

$$M = \frac{f_t}{f_o} \tag{3.4}$$

However, the magnification of an incorrectly aligned microscope, such as when the objective lens is not at the correct working distance, will differ from equation (3.4). This is because when $d\_sample \neq f_o$ an image can only be formed when $d\_cam \neq f_t$. The first step in our calibration routine is therefore to calculate the magnification for each channel for a range of suitable d_sample values, centred around the real effective focal length of the objective lens, f_o. To do this calculation, we substitute equation (3.2) into equation (3.1), set a value for d_sample from the range chosen as appropriate for the objective, and solve for the value of d_cam that gives an image at the sensor. This is easily done by recalling that the B component of the ABCD matrix of a system is equal to zero for systems producing a real image at the output plane from an object at the input plane. Therefore, a function that returns the value of B for a given physical setup can be passed to, e.g. the Python fsolve routine allowing a numerical solution for the

value of *d_cam* that produces an image for each *d_sample* in the range of interest. Note that it is possible that no imaging solution can be found, given the fixed camera position and the choice of *d_sample* range. In this case, our example code fails gracefully and warns the user of the position at which the failure occurs for the relevant path.

Substituting the solved *d_cam* value for each *d_sample* value back into the matrix equation allows the lateral magnification *A* to be determined for each iteration. A plot of lateral magnification vs *d_sample* shows the deviation in magnification when the objective lens is moved away from the correct working distance. For a multichannel microscope, repeating the analysis for each channel allows the theoretical difference in magnification between each channel to be modelled in the situation where the objective lens is not positioned correctly along the optical path. Note that the fundamental design choice that creates the differing magnification is the different path lengths for each channel. As such, if the microscope is designed with equal path lengths, it may be worthwhile to introduce a temporary path difference to allow alignment using this method. Since both arms will then be set up after alignment to image at the correct working distance, the path difference can be subsequently removed from the modified arm and that arm corrected relative to the unmodified arm.

The theoretical plot of lateral magnification versus *d_sample* can be used to align the position of the objective lens and tube lenses in an infinite-conjugate microscope. For a single channel microscope, the practical magnification of the microscope can be measured using, for example, a graticule sample. Then using this value, *d_sample* can be interpolated from the theoretical plot (example plot shown in figure 5). The difference in distance between *d_sample* and f_o is the distance the objective lens needs to move to be at the correct working distance and thus correcting the magnification of the microscope to the expected value.

We focus here, however, on alignment of multichannel infinite-conjugate microscopes in the case where a calibration sample, such as a graticule, may not be available. In this case, a plot of the modelled lateral magnification versus *d_sample* for each channel is created and then, so as to mitigate the need to measure true magnifications, each plot is normalized to a single channel (we select the channel with the shortest path length for consistency) to create a plot of normalized magnification versus *d_sample* for each channel. An example of the plots is given in figure 6 for a multichannel microscope with three channels where the path lengths of each channel are *d_total* = 300, 350 and 400 mm, respectively. All three channels are otherwise identical in terms of cameras and tube lenses. The camera specification of note is the pixel size; we measure the size of identifiable features within the image, and from there, estimate the relative magnification for each channel, using image pixel distances. Therefore, different-sized camera pixels will be measuring different absolute distances on the imaging plane and must be compensated for when comparing images from different pixel-sized cameras in the same microscope.

Note here that it can be seen that at the point where *d_sample* = f_o = 4.5 mm, the three channels have equal magnifications as expected. Then, as the objective lens is moved away from the correct position, the magnifications vary from one another. When the objective lens is too close to the sample (*d_sample* < 4.5 mm) the third channel has the smallest magnification. Whereas the first channel has the smallest magnification when the objective lens is too far away from the sample (*d_sample* > 4.5 mm). This allows unambiguous estimation of both the magnitude and direction of a positioning error of the sample plane.

To use the calculated plots for a multichannel infinite-conjugate microscope to align the objective lens and tube lenses the following steps are followed:

(i) Set up the microscope with each channel in focus, with the objective lens at a reasonable estimated working distance.
(ii) Capture an image on each channel of a sample where the distance in pixels between the same two points can be measured (a specific calibration slide allows absolute magnifica-
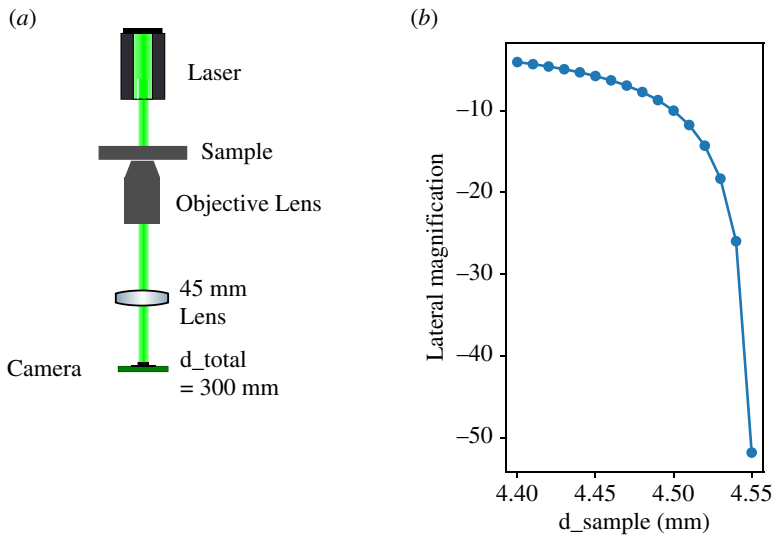
Figure 5. (*a*) Schematic of a single channel infinite-conjugate microscope. Figure from [2]. (*b*) Plot of lateral magnification versus *d_sample* created using our ray transfer matrix model for an infinite-conjugate microscope, setting *d_total* to 400 mm, f_o to 4.5 mm and f_t to 45 mm.
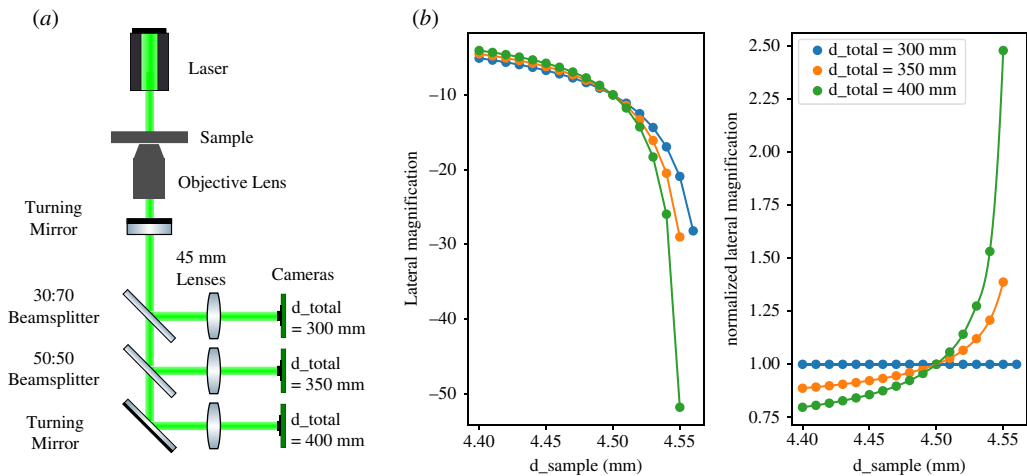

Figure 6. (*a*) Schematic of three-channel infinite-conjugate microscope. Figure from [2]. (*b*) Plots of lateral magnification and normalized lateral magnification versus *d_sample* created using our ray transfer matrix model for a three-channel infinite-conjugate microscope, setting *d_total* to 300, 350 and 400 mm, f_o to 4.5 mm and f_t to 45 mm for each channel.

tions to be calibrated and measured, while a general sample will allow for alignment but not confirm the final magnification).

(iii) Normalize the distances measured on the calibration images to the distance measured on the channel which was used for the lateral magnification normalization calculations.

(iv) To determine the predicted error in the position of the objective lens, the measured normalized magnification value for the channel with the largest *d_total* value, can be plotted on the normalized magnification graph and the corresponding *d_sample* value can be interpolated, which we define as *d_sample_interpolated*. The error in the position of the objective lens is then calculated according to equation (3.5). If the working distance error is a positive value, then the objective lens is that magnitude too far away from the sample, and if it is a negative value then it is that magnitude too close to the sample.

(v) The objective lens is then re-positioned using the microscope's objective lens focusing control using the correction obtained in step (iv). This underlines the need, mentioned in the introduction, for a method of accurately controlling z steps within the microscope imaging system. Moving the objective will defocus the image on the camera: the tube lens should then be moved to refocus the image. Note again that in this example the sample and camera positions are fixed.

(vi) The calibration process, starting at step (ii), can then be repeated, taking new images of the sample again to check the updated position of the objective lens. Depending on the tolerances of the microscope the routine may need repeated more than once.

$$working\ distance\ error = d\_sample\_interpolated - f_o \qquad (3.5)$$

There are some considerations to be made with this approach. Since we are normalizing distances relative to an ideal system, we are making some important assumptions, e.g. all lenses have the design focal length with no consideration of manufacturing tolerances. As such, there are a few areas where it is worth applying a critical approach when working with this alignment algorithm. Large discrepancies in the estimated current value of d_sample between different channels could indicate some of the following issues:

— The measurement of the feature size within the image implicitly assumes an image with no distortions. To minimize the impact of any distortions that are present, try to get feature size measurement from a region central to the image in case the magnification differs over the field of view (typical with high magnification, very simple optical systems). This is the easiest problem to test for, since it just requires repeating the computational side of the alignment, without needing new images.

— Tolerance differences on tube lenses (a 45 mm nominal focal length lens might have a different focal length as manufactured) are the final source of error we consider. This is likely the source of absolute errors on calibration (when all paths agree on the magnification, but it differs from the expected magnification, or when the calculated d_sample position is significantly different on each path). It is slightly more likely to be observed when a range of different tube lenses are used (e.g. same focal lengths but different lens types or different focal lengths to suit different cameras). This is the hardest to ascertain on a purely image-based system of calibration—it may be that testing of the focal length is required for each lens.

Finally, we note that the use of normalized magnification also allows the alignment of channels that have different absolute magnifications and/or cameras with differing pixel sizes. If the normalization is performed over both relative magnification and relative pixel size, then the error in d_sample can still be estimated. See our sample code for an example of how to implement this normalization.

4. Practical examples

To show the alignment procedure works in practice, we used the M4All fluorescence and transport of intensity equation (TIE) microscope (figure 3), which as mentioned in §1 combines the M4All system [12] and the OpenFlexure microscope stage [10]. Full build instructions can be found on the M4All repository [12]. This configuration of the M4All microscope was designed for single channel fluorescence and simultaneous brightfield multifocal plane imaging to enable computational phase contrast microscopy using the TIE [15,16], requiring a total of four channels which need to be correctly aligned. While the correct alignment of the focal plane offset in a multi-focal microscope is beyond the scope of this paper, it can be seen that the configuration provides an ideal system in which we can demonstrate the effectiveness of the RTMA alignment procedure. A schematic of the microscope can be seen in figure 3*a* along with photos of the microscope in figure 3*b,c*.
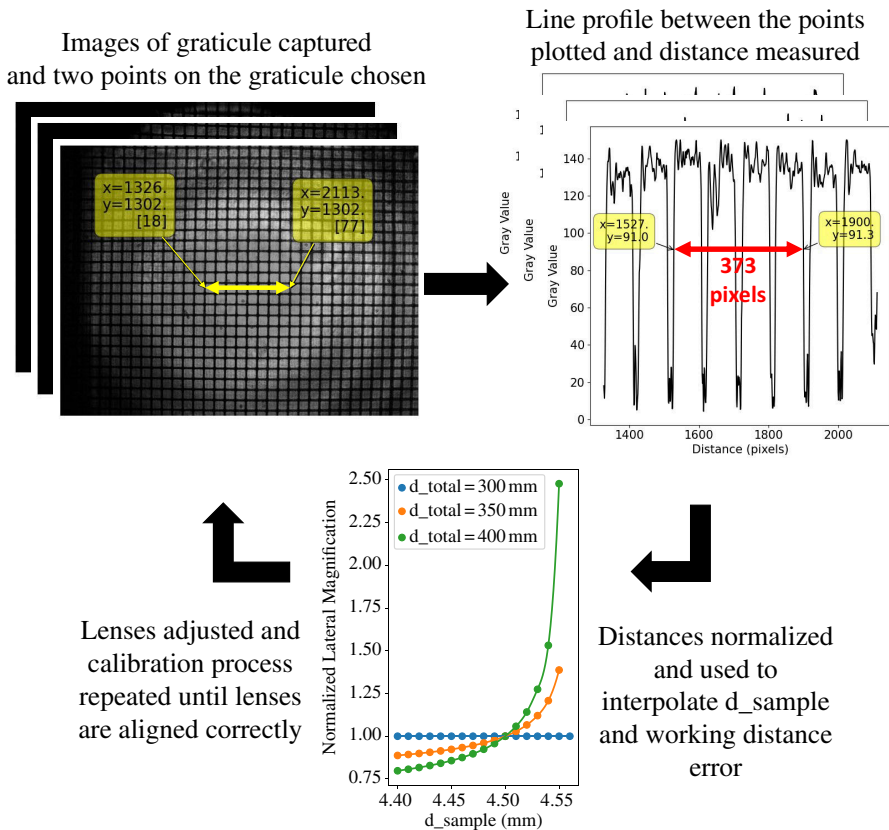
Figure 7. Outline of alignment process steps where an image of a 10 μm graticule is captured on each channel. Next, a line profile is plotted for each image and the distance between the same number of grid squares is measured in pixels. The distances are then normalized and the plot of lateral magnification versus *d_sample* obtained from the ray transfer matrix analysis model is used to interpolate *d_sample* and thus the objective lens' working distance error. Finally, the lenses are re-positioned and the alignment process is repeated until the lenses are aligned. Figure adapted from [2].

A turning mirror (Thorlabs PF10-03-P01) placed below the OpenFlexure microscope stage couples the light into the M4All cubes. A 650 nm shortpass dichroic mirror (Thorlabs DMSP650) then reflects fluorescence emission ≥650 nm which is focused by a 125 mm focal length tube lens (Thorlabs AC254-125-A) onto an IDS CMOS camera (UI-3060CP-M-GL Rev. 2). The remaining transmitted laser light is split into the three brightfield channels by 30:70 and 50:50 beamsplitters (Thorlabs BSS10R and BSW10R) and focused by 45 mm focal length tube lenses (Thorlabs AC254-045-A) onto Raspberry Pi v2 camera modules. The three tube lenses in the brightfield channels would normally be focused on different *z* planes to enable multifocal plane imaging. However, before altering the positions of the three brightfield channel tube lenses to enable multifocal plane imaging for future work, it is necessary to ensure that the overall alignment and collimation of the infinity space of the microscope is correct, so we first used the ray transfer matrix alignment method to co-align each channel to image the same plane at the correct working distance. The three brightfield channels have the same *d_total* values of 300, 350 and 400 mm as the example in figure 6.

We first set the microscope up with each brightfield channel in focus and captured an image of a 10 μm graticule sample (Pyser-SGI S29 grid, order code 02B00429, though other S29 calibration slides are available from a range of suppliers). As discussed above, it is worth emphasizing that any sample where the distance in pixels between the same two feature points can be measured for every channel can be used when absolute magnification calibration is not
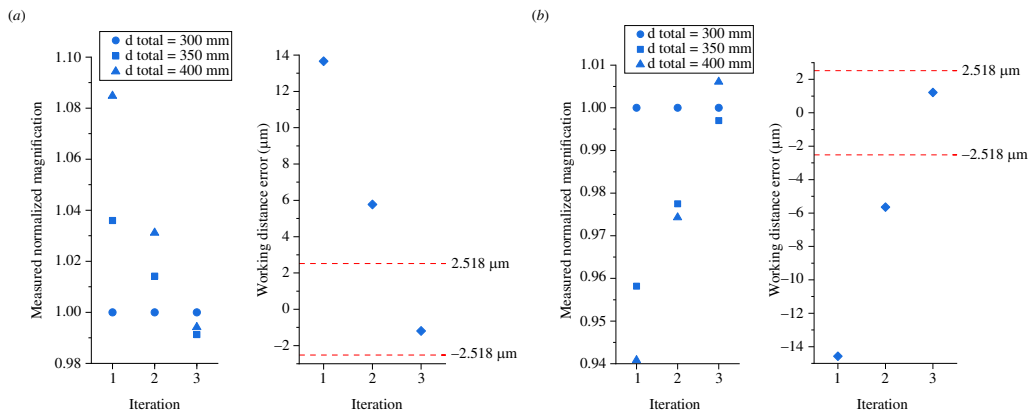
Figure 8. Calibration procedure results showing the measured normalized magnifications and the working distance errors for the situations where (*a*) the objective lens was intentionally positioned too far away from the sample and (*b*) too close to the sample. The red dashed lines on the working distance error graphs indicate the axial resolution limit of the M4All Fluorescence and TIE microscope, calculated using Abbe's axial resolution equation. Figure adapted from [2].

required. An example of such a slide would be sparse fluorescent or metallic beads distributed on a coverslip and appropriately mounted. As we were using a graticule, a line profile of the graticule was plotted for each channel and the distance in pixels between the same two points on each plot was measured. The distances were then normalized to the first brightfield channel (*d_total* = 300 mm), which we call the measured normalized magnifications, and used to interpolate *d_sample* from the plot of normalized lateral magnification versus *d_sample* in figure 6*b*. The working distance error was then calculated from equation (3.5). A flow chart of the alignment steps is given in figure 7.

The alignment process was then iterated until the three channels had equal magnifications within the tolerances of the equipment and *d_sample* = f_o within the optical axial resolution limit (d_z). For this example microscope, the wavelength of light, λ, was 532 nm, and the numerical aperture, *NA*, of the objective lens was 0.65, resulting in an axial resolution limit of 2.518 μm using Abbe's axial diffraction equation, $d_z = 2\lambda/NA^2$. We carried out the alignment process for the situation where the initial position of the objective lens was intentionally too far away from the sample, and again when it was too close to the sample. The results are shown in figure 8. In both the cases shown, it took three iterations of the alignment process to reduce the working distance error to less than the axial resolution limit (indicated by the red dashed lines on the working distance error graphs). Repeats for intentional misalignment of the objective lens and performing the alignment procedure can be found in electronic supplementary material, figure S1. Please note, for transparency, the data in figure 8 were obtained using an older version of our code where the RTMA model computations were performed using Maple™ (Maple is a trademark of Waterloo Maple Inc.) and the magnification analysis was performed in a Jupyter Notebook, both of which are provided as electronic supplemental material [17]. We have since written both the RTMA model and analysis code in a single Jupyter Notebook which gives equivalent results and is also provided. The magnification plots in figures 5 and 6 were created using our new code.

5. Conclusion

RTMA within the paraxial approximation has been shown to effectively model the lateral magnifications of the imaging paths in a multichannel infinite-conjugate microscope when

13

royalsocietypublishing.org/journal/rsta   *Phil. Trans. R. Soc. A* **382:** 20230107

the optics are both aligned and misaligned along the optical axis. Furthermore, we have shown how magnification measurements from images acquired on each channel can be used to interpolate objective lens position from the model and how this information can be used to practically align the microscope optics. We have validated this alignment method on an open-source 3D printed multichannel microscope and shown it is a powerful tool when use of additional alignment hardware is not suitable (however, the method is applicable to all multi-channel infinite-conjugate imaging systems). We provide the Python code for the RTMA model and alignment algorithm as a detailed open-source Jupyter Notebook and believe it will be a useful tool for the open-source microscopy hardware community.

References

1. Sanderson J. 2019 Basic microscope optics. In *Understanding light microscopy* pp. 55–74. John Wiley & Sons, Ltd. (doi:10.1002/9781118696736)
2. Cairns GS. 2022 Development of microscopy hardware & imaging techniques for macrophage host defence research. Doctoral Thesis, University of Strathclyde. See https://doi.org/10.48730/yc8y-wj70
3. Sanderson J. 2019 The microscope objective. In *Understanding light microscopy* pp. 127–160. John Wiley & Sons, Ltd. (doi:10.1002/9781118696736)
4. Valérie Pineau N, Shadi M, Elahe P, Gabriel G, Ludovick B, Marc-André V, Daniel CC. 2021 Tools and tutorial on practical ray tracing for microscopy. *Neurophotonics* **8**, 010801. (doi:10.1117/1.NPh.8.1.010801)
5. HohlbeinLab. 2022 HohlbeinLab/OpenMicroscopy/OM_Hardware https://github.com/HohlbeinLab/OpenMicroscopy/blob/main/ src/OM_Hardware.md
6. Johnstone G, Patton B. 2022 Using an autocollimator to align 4f systems. See https://doi.org/10.1242/focalplane.11048
7. OpenRAMAN. *OpenRAMAN*. See https://www.open-raman.org/.
8. The Pulsar. 2017 *Building an Autocollimator for the Lab*. See https://www.thepulsar.be/article/building-an-autocollimator-for-the-lab/.
9. The Pulsar. 2015 *A reference of optical infinity*. See https://www.thepulsar.be/article/a-reference-of-optical-infinity/.
10. Sharkey JP, Foo DCW, Kabla A, Baumberg JJ, Bowman RW. 2016 A one-piece 3D printed flexure translation stage for open-source microscopy. *Rev. Sci. Instrum.* **87**, 025104. (doi:10.1063/1.4941068)
11. Heintzmann R. 2013 A appendix: practical guide to optical alignment. In *Fluorescence microscopy* pp. 393–401. (doi:10.1002/9783527671595)
12. Cairns GS. 2021 NanoBioPhotonics-Strathclyde/M4All. See https://doi.org/10.5281/zenodo.5569711

13. FreeCAD. 2019 See https://github.com/FreeCAD/FreeCAD/releases/tag/0.18.4.
14. Gerrard A, Burch JM. 1994 *Introduction to matrix methods in optics*. New York: Dover.
15. Davis QT. 2017 Transport of intensity equation microscopy for dynamic microtubules. See https://arxiv.org/abs/1707.04139
16. Grant SD, Richford K, Burdett HL, McKee D, Patton BR. 2020 Low-cost, open-access quantitative phase imaging of algal cells using the transport of intensity equation. *R. Soc. Open Sci.* **7**, 191921. (doi:10.1098/rsos.191921)
17. Cairns GS, Patton BR. 2023 Data and code for: An open-source alignment method for multichannel infinite-conjugate microscopes using a ray transfer matrix analysis model. Zenodo. https://zenodo.org/records/8125286
18. Cairns GS, Patton BR. 2024 Supplementary material from: An open-source alignment method for multichannel infinite-conjugate microscopes using a ray transfer matrix analysis model. Figshare. (doi:10.6084/m9.figshare.c.7200898)